Citation: I. Cuiral-Zueco, G. López-Nicolás, H. Araujo. Gripper positioning for object deformation tasks. IEEE International Conference on Robotics and Automation (ICRA), pp. 963-969. Philadelphia (PA), USA, May 23-27, 2022.

Gripper positioning for object deformation tasks

Ignacio Cuiral-Zueco, Gonzalo López-Nicolás and Helder Araujo

***Abstract*— Shape control involves bringing a deformable object to a desired shape. In the shape control literature, the positioning of the grippers on the object is usually predefined (user-defined) and therefore considered as input information. In this paper we address the gripper positioning problem for shape control. We propose a deformation process within a simulated fully-actuated scenario and introduce multi-scale centroid paths as geometry describing points for which we prove individual control feasibility. Analysis on the evolution of multi-scale centroid paths through the fully-actuated deformation process allows us to define an importance metric for gripper candidates. Final gripper positions, based on the importance metric, are obtained through optimisation. We present simulation results for global and local shape control problems.**

I. INTRODUCTION

Shape control is an emerging branch of control engineering that deals with the problem of bringing a deformable object to a desired target shape with the use of robotic manipulators (further formalisation of the problem in surveys [1], [2]). Several works tackle deformation tasks from different perspectives (for example [3]–[5] for shape control or [6] for deformable object cutting). However, they share a common factor: the positioning of the grippers on the object is predefined (user-defined) and is therefore given as input to the problem. A poor gripper setup may lead to the non-feasibility of the deformation task, i.e., a good gripper positioning may not only improve the control strategy performance, but may also be decisive for the task's feasibility (the importance of gripper positioning is illustrated in the in the accompanying video). For a deformable object to be fully actuated, within the context of shape control, there should be a gripper positioned at every point along the object. Unfortunately, a fully actuated system is not feasible in real setups as it would require a very high number of grippers. Even the discrete approximation, involving a large number of grippers, would be problematic for a variety of reasons, namely: lack of robot availability or incompatible robot work-spaces (collisions). These issues give rise to the definition of the problem addressed in this paper. This problem addresses location of grippers along the object to get the most out of the available number of grippers in an specific shape control task.

I. Cuiral-Zueco and G. López-Nicolás are with Instituto de Investigación en Ingeniería de Aragón, Universidad de Zaragoza, Spain (ignaciocuiral@unizar.es, gonlopez@unizar.es).
H. Araujo is with the Institute for Systems and Robotics, Universidade de Coimbra, Portugal (helder@isr.uc.pt).

This work was supported by the Spanish Government/European Union through projects PGC2018-098719-B-I00 (MCIU/AEI/FEDER, UE) and COMMANDIA SOE2/P1/F0638 (Interreg Sudoe Programme, ERDF), and DGA_T45-20R (Gobierno de Aragón), and by Fundação para a Ciência e a Tecnologia (FCT) by project UIDB/00048/2020.

A. Related work

Within the non-rigid object context, a distinction should be made between two research lines that, while sharing certain similarities, focus on different problems: the grasp quality problem and gripper positioning for deformation. The former solves the problem of grip stability [7] and actions performed with robotic hands on objects with a size similar to that of the grasping hand. The latter assumes the grasping problem is solved. It rather focuses on solving the strategic gripper locations on large objects (generally larger than the gripper size) to perform collaborative tasks such as object transport or shape control. This problem classification is presented in [8], where a method for in-hand shaping of non-rigid objects is presented along with a contact-point selection criterion. Regarding the second problem (gripper positioning) and focusing on cloth grasping, [9] uses non-linear SVM on 3D visual information and defines a criterion for selecting the best grasping point. Tackling a similar problem: robot-assisted dressing, [10] proposes a supervised deep neural network trained with synthetic datasets to perform grasping-point prediction and collaborative manipulation. However, none of these approaches consider the shape control task, as they focus on very specific textile applications (mainly transport or folding) and single-gripper scenarios. Our proposal considers a multi-gripper scenario and adopts an optimisation approach closer to those defined in multi-agent robot systems [11] [12]. For example, [13] proposes a hybrid centralised/distributed multi-robot deformable object manipulation method. Proposal in [14] adopts a multi-agent strategy for shape control and transport but the gripper positioning problem is trivially solved by placing equidistant grippers along the contour. A similar gripper distribution is adopted in the shape control proposal defined in [15]. To our knowledge, there are no previous approaches that focus on gripper positioning for collaborative deformable object shape control.

B. Proposal approach overview

In this paper, we tackle the gripper positioning problem for shape control by means of multiple robots with grippers. Our approach consists of three main blocks (Fig. 1). In the first one, we define a reference deformation process considering a fully-actuated scenario. This provides us with a desirable shape evolution of the object into the target shape. In the second block we describe the error metric that is going to define the importance of every contour point as a gripper candidate. This error metric, based on geometric multi-scale centroid paths (described in section III), is going to be computed along iterations using the information provided by

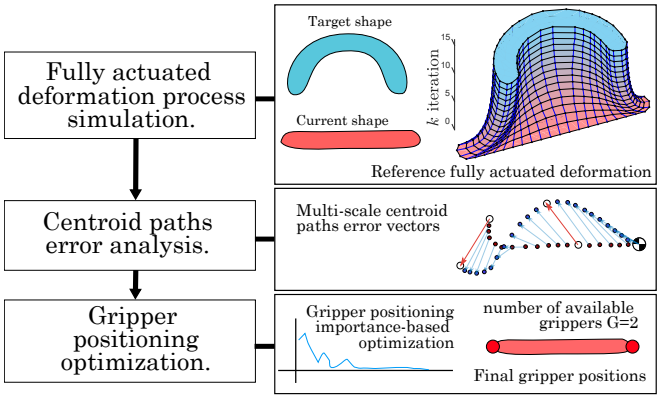

Fig. 1: Proposed approach overview scheme. On the left, the main three blocks of the method. On the right, representative illustrations of each block.

the reference deformation process. The output of the second block is a gripper-importance array that serves as input in the optimisation process in block three.

C. Problem formulation

Regarding the object to be deformed, we assume its geometry is planar and there is no prior knowledge of its physical properties (Young modulus, stiffness, etc). Our proposal considers that the object's surface may lack texture (i.e. we cannot rely on texture-based visual descriptors). Then, the available object information consists of a set of points of the object's visible surface (as it would be obtained with the use of an RGB-D visual sensor). We also assume that the surface of the object remains visible during the deformation process, something that could be achieved with optimal perception methods [16]. We define the object's shape as its visible 2D surface (embedded in 3D Euclidean space). As for the grippers, the number of available grippers is $\mathrm{G} \geq 2$. At least two grippers are required in order to cause any deformation on a steady-state deformable object when inertia and gravity are negligible (a common assumption in the shape control literature, for instance [3] and [17]). We also assume that modifying gripper-to-object contact points would hamper the shape control process and thus these will not be modified during the deformation process.

For the problem setup, consider the set of points $v_n \in V = \{v_n, n = 1, \ldots, N\}$ in 3D space that represent the discretised visible 2D surface of the object in its current state (represented in Fig. 2). Within this set, an α-shape contour extraction retrieves the boundary points $v_m^b \in V^b = \{v_m, m = 1, \ldots, M\}$ such that $V^b \subseteq V$. We will focus the search of the best gripper points on the object contour. Therefore, the set of contour points V^b defines the solution space, and each of the contour points v_m^b becomes a candidate for gripper positioning. We define the discretised target shape surface with points $\bar{v}_p \in \bar{V} = \{\bar{v}_p, p = 1, \ldots, P\}$ and the target boundary subset $\bar{v}_q^b \in \bar{V}^b = \{\bar{v}_q^b, q = 1, \ldots, Q\}$, being $\bar{V}^b \subseteq \bar{V}$ and thus $Q \leq P$. Current contour points v_m^b and target contour points $\bar{v}_q^b$ are elastically matched at each

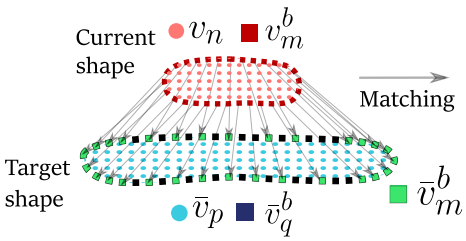

Fig. 2: Example of elastic contour matching, on which points from the current shape v_m^b contour are elastically matched at each step [18] to points on the target contour $\bar{v}_m^b$.

simulation step using a multi-scale Laplacian-based FMM [18]. The elastic matching assigns a target contour point $\bar{v}_m^b \in \bar{V}^b$ to each current contour point v_m^b. Note that this matching is elastic and not necessarily homogeneous as it maximises shape resemblance on a multi-scale level.

II. FULLY-ACTUATED DEFORMATION SCENARIO

One of the main problems that arise on shape control is the lack of analysis along time. Methods need to rely on local stability and local convergence. This complicates the gripper positioning process: a position may not appear to be important at the beginning of the deformation process but may be of great relevance at a later stage. One might suggest modifying the positioning of the grippers throughout the deformation process, but this would not only be problematic in practice but would also add additional complexity to the shape control strategy design.

Considering the time-locality perspective problem, we propose a deformation process within a fully-actuated scenario (see the shape evolution simulation example in Fig. 1, top right corner). The deformation that results from the simulation steps is just one of the infinite possibilities (or *deformation paths*) the object can take in order to reach the target shape. However, this path in particular has three characteristics that make it geometrically convenient:

1) **Fully-actuated system:** in the simulation we assume an all-gripper configuration, this means $\forall v_m^b \in V^b \, \exists \gamma_g \in \Gamma$ such that $v_m^b \equiv \gamma_g$. Being $\Gamma = \{\gamma_g, g = 1, ..., \mathrm{G}\}$ the set of grippers γ_g for which control actions $\mathbf{u}_g \in \mathbb{R}^3$ are defined. Note that, in this fully-actuated approximation, $G = M$. We define $\boldsymbol{\gamma}_g \in \mathbb{R}^3$ as the position vector of γ_g. Each of the discrete contour points v_m^b can be actuated with a single integrator model $\dot{\boldsymbol{\gamma}}_g = \mathbf{u}_g$.

2) **Laplacian-based elastic matching:** The elastic matching between the current and the target shape is performed at each step [18]. This optimises the shape resemblance on a multi-scale level and thus minimises deformation energy.

3) **Gripper action minimisation:** The action of each gripper $\mathbf{u}_g$ is defined by its position error vector with respect to its corresponding target point. A Procrustes optimisation process applies a rigid transform to the target points and minimises the point-to-point overall distance. This results in an action energy minimisation.

It is important to mention that this reference deformation process does not require to simulate the physics behaviour of the object as it is merely geometrical. This fact implies the need of assuming the object is behaving in a compliant way under actions $\mathbf{u}_g$.

III. MULTI-SCALE CENTROID PATHS

A. The relevance of multi-scale centroids on shape control

Consider a planar deformable object in stationary state (Fig. 3.1). One of its contour points v^b_{fixed} is position-constrained (i.e. passive gripper in relative terms, recall $G \geq 2$). There is also an active gripper $\gamma_g \equiv v^b_m$. Now consider a region Ω of the object such that its points lie within a topological distance s from v^b_m. Following some user-defined deformation task, we want to move the geometric centroid c_m of region Ω to a target point $\bar{c}_m$. The error vector is defined as $\mathbf{e}_m = \bar{\mathbf{c}}_m - \mathbf{c}_m$, where $\mathbf{c}_m$ and $\bar{\mathbf{c}}_m$ denote the position vectors of c_m and $\bar{c}_m$ respectively. Assuming planar deformation, we define a reference frame $\mathcal{F}$ with origin at v^b_{fixed}, X-axis always pointing towards v^b_m ($\mathcal{F}$ rotates jointly with v^b_m) and Y-axis is co-planar to the deformation plane. Note that $\mathcal{F}$ allows to define object coordinates in 2D (intrinsic coordinates). Vector $\mathbf{v} = (v^b_{mx}, 0), v^b_{mx} > 0$ defines the position of v^b_m in $\mathcal{F}$'s reference frame. Considering v^b_{fixed} constitutes a free-rotating point, and disregarding momentum dissipation along the object, a tangent velocity action $\mathbf{u}^\theta_g$ on v^b_m generates a rotation θ with respect to v^b_{fixed} on all object points (Fig. 3.2). This means that the geometric centroid c_m of any region Ω will rotate the same angle θ with respect to v^b_{fixed}. On the other hand, an action $\mathbf{u}^\mathbf{v}_g = (u^\mathbf{v}_{g_x}, 0)$ on v^b_m generates a velocity vector field in all object points that have positive x coordinates (again, disregarding energy dissipation, i.e. the vector field of the velocity does not decay except by its own definition). This vector field represents the stretching or compressing process of the object and applies an affine transformation $\mathbf{T} \in \mathbb{R}^{2\times 2}$ on points with positive x coordinates. We define $\mathbf{T}$ in $\mathcal{F}$ coordinates:

$$\mathbf{T} = \begin{bmatrix} \frac{v^b_{mx} + u^\mathbf{v}_{g_x}}{v^b_{mx}} & 0 \\ 0 & 1 \end{bmatrix}, \tag{1}$$

with determinant $|T| = 1 + u^\mathbf{v}_{g_x}/v^b_{mx}$ and $v^b_{mx} > 0$ (recall the definition of $\mathcal{F}$). We assume $v^b_{mx} + u^\mathbf{v}_{g_x} > 0$ as to prevent flipping the points of the object. With these considerations, $|T|$ satisfies $|T| > 0$ and provides a ratio of area variation for differential surface elements. When $|T| < 1$, the object is being compressed in the X direction. Similarly, $|T| > 1$ implies a stretching process on the direction of the X axis. The centroid of a differential element of surface at some point $\mathbf{x}$ is $\mathbf{c}_d = [x + dx/2, y + dy/2]^\intercal$. The change on $\mathbf{c}_d$ after applying the $\mathbf{T}$ transform yields:

$$\dot{\mathbf{c}}_d = \mathbf{T}\mathbf{c}_d - \mathbf{c}_d = \begin{bmatrix} \frac{u^\mathbf{v}_{g_x}}{v^b_{mx}}(x + \frac{dx}{2}) \\ 0 \end{bmatrix}. \tag{2}$$

In any region Ω, given that $\exists \mathbf{x} \in \Omega$ such that $x > 0$, all surface differential elements with $x > 0$ contribute in moving the centroid c_m of the region in the direction of $\mathbf{u}^\mathbf{v}_g$.

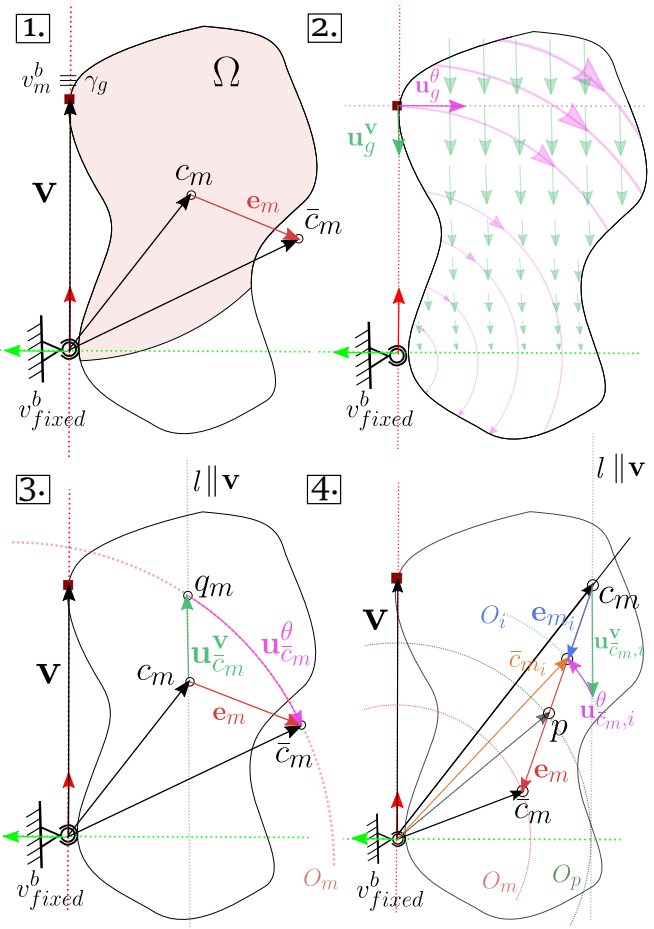

Fig. 3: 1. shows elements that define the centroid control problem. Amongst them, error $\mathbf{e}_m$: defined from c_m to $\bar{c}_m$. In 2. the velocity vector fields generated by actions $\mathbf{u}^\mathbf{v}_g$ and $\mathbf{u}^\theta_g$ can be visualised. 3. and 4. provide examples that illustrate how control actions $\mathbf{u}^\mathbf{v}_{\bar{c}_m}$, $\mathbf{u}^\theta_{\bar{c}_m}$ and $\mathbf{u}^\mathbf{v}_{\bar{c}_{m,i}}$,$\mathbf{u}^\theta_{\bar{c}_{m,i}}$ can be applied consecutively to reduce error $\mathbf{e}_m$.

So far we defined two generic actions $\mathbf{u}^\theta_g$ and $\mathbf{u}^\mathbf{v}_g$ on v^b_m. Action $\mathbf{u}^\theta_g$ allows us to control the rotation of c_m in any given configuration. However, in order for $\mathbf{u}^\mathbf{v}_g$ to control the position of c_m in the direction of X, two conditions must be satisfied: 1) $\exists \mathbf{x} \in \Omega$ such that $x > 0$, and 2) $v^b_{mx} + u^\mathbf{v}_{g_x} > 0$. For the moment, let us assume both conditions are satisfied. We define circle O_m centred at $\mathcal{F}$'s origin with radius $r_m = \|\bar{\mathbf{c}}_m\|$ (Fig. 3.3). When $\|\bar{\mathbf{c}}_m\| \geq \|\mathbf{c}_m\|$, c_m is contained within O_m. This means line $l = \mathbf{c}_m + t\hat{\mathbf{v}}, t \in \mathbb{R}$ ($\hat{\mathbf{v}}$ being the unitary vector in the direction of $\mathbf{v}$), will always intersect O_m in, at least, one point q_m. This allows to define the control law: $\mathbf{u}^\mathbf{v}_g = \alpha \mathbf{u}^\mathbf{v}_{\bar{c}_m}$, $\mathbf{u}^\theta_g = \alpha \mathbf{u}^\theta_{\bar{c}_m}$, where $0 < \alpha \leq 1$ is the control gain. Vector $\mathbf{u}^\mathbf{v}_{\bar{c}_m}$ defines the position error of the intersection point q_m along line l (if there are two intersection points, q_m is the closest to $\bar{c}_m$). Similarly, $\mathbf{u}^\theta_{\bar{c}_m}$ defines the angular error along circle O_m. The consecutive execution of these control actions brings c_m to $\bar{c}_m$, which leads to the reduction of error $\mathbf{e}_m$. Things get more complicated when $\|\bar{\mathbf{c}}_m\| < \|\mathbf{c}_m\|$ as the intersection of

line l with circle O_m is not ensured (Fig. 3.4). Considering this, the condition for the intersection to happen is $r_m \geq \|\mathbf{c}_{m_y}\|$. We can define a circle O_p with $r_p = \|\mathbf{c}_{m_y}\|$ that satisfies this condition. Circle O_p intersects the error vector $\mathbf{e}_m$ at point p. Point p and c_m define vector $\mathbf{e}_{m_p} = b\,\mathbf{e}_m$, with $b \in \mathbb{R}, 0 < b < 1$. Note that O_i infinite circles can be defined with $r_i \in [r_p, \|\mathbf{c}_m\|)$, $i \in \mathbb{N}$. All of these circles generate intersections $\bar{c}_{m_i}$ with $\mathbf{e}_m$. The intersections lie between c_m and p and provide infinite reachable target points and thus reducible error vectors $\mathbf{e}_{m_i}$ in the direction of the error $\mathbf{e}_m$. Generalising, regardless of $\|\bar{\mathbf{c}}_m\|$ and $\|\mathbf{c}_m\|$, a circle O_i centred at $(0,0)$ can be always defined in such a way that its intersection with $\mathbf{e}_m$ generates a reachable target point $\bar{c}_{m_i}$. Control laws:

$$\mathbf{u}_g^{\mathbf{v}} = \alpha \mathbf{u}_{\bar{c}_m,i}^{\mathbf{v}}\,, \quad \mathbf{u}_g^{\theta} = \alpha \mathbf{u}_{\bar{c}_m,i}^{\theta} \tag{3}$$

applied consecutively, move c_m in the direction of $\mathbf{e}_{m_i} = a\,\mathbf{e}_m$ (with $a \in \mathbb{R}$, $0 < a \leq b$) and thus reduce error $\mathbf{e}_m$. Since point v_m^b, by definition, is always going to be within Ω and $v_{mx}^b > 0$, condition 1: $\exists\, \mathbf{x} \in \Omega$ such that $x > 0$ is always satisfied. On the other hand, for larger values of r_i, both $\|\mathbf{e}_{m_i}\|$ and $\|\mathbf{u}_{\bar{c}_m,i}^{\mathbf{v}}\|$ decrease. Regarding that $\mathbf{e}_{m_i} = a\mathbf{e}_m$, one can always find a larger r_i that results in a sufficiently small $a > 0$ so that $\mathbf{u}_{\bar{c}_m,i}^{\mathbf{v}}$ generates an action $\mathbf{u}_g^{\mathbf{v}}$ such that $u_{g_x}^{\mathbf{v}} < v_{mx}^b$ and thus condition 2: $v_{mx}^b + u_{g_x}^{\mathbf{v}} > 0$ can be always satisfied.

Recall Ω is defined by the topological distance s. When $s = 0$, centroid c_m is equivalent to v_m^b. Similarly, when $s = s_{max}$ (s_{max} is the maximum topological distance within the object) centroid c_m is equivalent to the global centroid of the object. A set of uniformly distributed distance values $s^\lambda \in S = \{s^\lambda, \lambda = 1, \ldots, \Lambda\}$, where $s^1 = 0$ and $s^\Lambda = s_{max}$, can be defined. For a contour point v_m^b, all centroids c_m^λ (generated with topological distances s^λ) constitute a multi-scale centroid path $C_m = \{c_m^\lambda, \lambda = 1, \ldots, \Lambda\}$ (See Fig. 4). Centroids within path C_m represent the group of shape-geometry describing points for which we can surely reduce position error, at least individually, with actions over contour point v_m^b and a fixed contour point v_{fixed}^b. Note that, since $G \geq 2$, there is always one gripper that can act as fixed gripper. Centroids defined with small s^λ values will describe smaller regions of the shape's geometry in finer detail, whereas centroids defined with large s^λ values will describe larger regions of the shape's geometry but in a more ambiguous manner. This fits the nature of deformable objects as the uncertainty of the action's effects on object points increases with distance to the actuator.

B. Multi-scale centroid path error and gripper importance

Contour point v_m^b has an assigned target point $\bar{v}_m^b$ with an associated multi-scale centroid path $\bar{C}_m$. A rigid translation (pure translation, no rotation) is applied to centroids in $\bar{C}_m$ such that $C_m^\Lambda \equiv \bar{C}_m^\Lambda$ (Fig. 5). This transformation is not arbitrary: in shape control, error vectors should not depend on the current and target object's relative positions. On the other hand, orientations at intermediate scales carry information

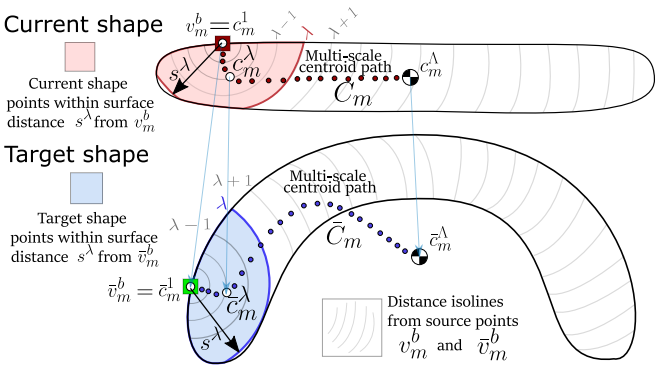

Fig. 4: Centroid error paths C_m and $\bar{C}_m$ for a current and a target shape are represented. Each path is defined by a series of centroids c_m^λ and $\bar{c}_m^\lambda$ defined at different scales λ.

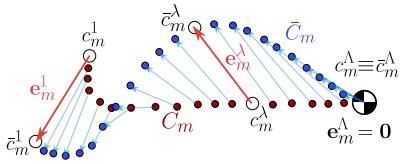

Fig. 5: Error vectors $\mathbf{e}_m^\lambda$ are defined for each centroid c_m^λ with their target centroids $\bar{c}_m^\lambda$.

about the object's shape and thus relative orientation between centroid paths should remain unchanged. Error vectors $\mathbf{e}_m^\lambda$ are defined for each centroid c_m^λ with their target centroids $\bar{c}_m^\lambda$. Maximum scale s^Λ takes the value of the largest s_{max} value amongst the current and the target shape. This means the shape with lowest s_{max} will have more than one centroid at C_m^Λ (or $\bar{C}_m^\Lambda$, given the case). This can be observed in Fig. 5, where several error vectors start from c_m^Λ.

Using the information of the fully-actuated simulation process we define the importance $w_m \in W = \{w_m, m = 1, \ldots, M\}$ of contour points v_m^b as gripper candidates with

$$w_m = \sum_{k=1}^{K} \sum_{\lambda=1}^{\Lambda(k)} \|\mathbf{e}_m^{\lambda(k)}(k)\|, \tag{4}$$

where $K \in \mathbb{N}$ are the number of iterations in the reference simulation. Larger values of w_m imply a more relevant position. From a shape control perspective, w_m contains the accumulated multi-scale centroid path error, in other words: it carries the information of the amount of error being perceived by contour point v_m^b during the reference deformation process. Contour points that do not perceive much error are not strategically located as they will not allow control laws to reduce a large amount of error.

IV. GRIPPER POSITIONING OPTIMISATION

Gripper importance values $w_m \in W$ (4) conform vector $\mathbf{w} \in \mathbb{R}^M$, $\mathbf{w} = [w_m]$. A local-maxima search on $\mathbf{w}$ selects the most relevant gripper candidates $v_j^b \in V^j = \{v_j^b, j = 1, \ldots, J\}$ such that $V^j \subseteq V^b$ (shown in green in the video). These relevant candidates have an associated

importance value of w_j. Vector $\boldsymbol{\tau} \in \mathbb{R}^J$, with elements $\tau_j = 1/w_j$, represents the assignation cost of each relevant gripper candidate v_j^b. Assignation costs in $\boldsymbol{\tau}$ are normalised as $\hat{\tau}_j = \tau_j / \max(\boldsymbol{\tau})$. A vector of booleans $\chi \in \mathbb{B}^J$ constitutes the decision variable of the optimisation:

$$\chi = \arg\min_{\chi} \left(\chi^\intercal \hat{\boldsymbol{\tau}} + \frac{\beta}{d_{max}} \left\| \frac{\chi^\intercal \mathbf{V}}{\chi^\intercal \chi} - (\mathbf{c}^\Lambda)^\intercal (k=1) \right\|_2 \right), \quad \text{subject to} \quad 2 \leq \chi^\intercal \chi = G. \tag{5}$$

If a gripper is positioned at v_j^b, the optimisation variable $\chi_j = 1$. Otherwise, χ_j takes the value of 0. The first term in the minimisation function represents the cost of assignations with respect to the gripper importance w_j. The second term penalises the distance between the centroid of the allocated grippers positions and the object's global centroid $\mathbf{c}^\Lambda(k = 1)$. Matrix $\mathbf{V} \in \mathbb{R}^{J\times 3}$ is obtained by stacking the position vectors $\mathbf{v}_j^b \in \mathbb{R}^3$ of v_j^b and d_{max} is the maximum distance from a contour point v_m^b to the object's global centroid at the initial instant $\mathbf{c}^\Lambda(k = 1)$. Although the centroid distance is normalised with d_{max}, it should be relevant only in the case of evenness of w_j. For this reason $\beta > 0$ is set to low values, in our simulations $\beta = 0.1$. The second term is designed to enhance the effectiveness of control actions as it favours uniformly distributed grippers. A more distributed gripper setup favours larger v_{mx}^b values and, since $v_{mx}^b + u_{g_x}^{\mathbf{v}} > 0$, it also allows larger velocity actions. The constraint in (5) guarantees that all available grippers G are allocated. Note that G should have values $G \leq J$, as J defines the size of the decision variable χ.

V. GRIPPER POSITIONING RESULTS

The method has been tested on several examples that range from local to global deformations and mixed global-local cases. Fig. 7 shows several of these examples, each row contains a specific shape control problem. The first column shows the shape-control problem to be solved. The contour of the current shape is shown in red and the contour of the target shape in blue. Both contours are connected with grey lines that represent the initial elastic contour matching (for $k = 1$). A Procrustes transform has been applied to the target shape in order to minimise matched-point distance. The second column illustrates the fully-actuated deformation process simulation. The evolution of the current shape through iterations can be visualised along the vertical-axis. The last two columns show the results results obtained by applying the grippers positioning method for different numbers of available grippers G. Contour points are plotted with circles of size proportional to their importance value w_m. Gripper-free contour points are represented in blue colour, whereas gripper positions are represented by red dots with overlapping crosses. The third column shows the results when a larger number of grippers G is selected, while the fourth column presents results for lower G values. A qualitative analysis of the results of each example is presented below. The first case represents a highly global case of deformation. A certain similarity can be found between the value of w_m of the current contour points (size of the blue circles on the last two columns) and the magnitude of the position error between assigned points $d_m = \|\bar{\mathbf{v}}_m^b(k = 1) - \mathbf{v}_m^b(k = 1)\|$ (length of the grey lines on the first column), being $\bar{\mathbf{v}}_m^b \in \mathbb{R}^3$ the target point's position vector. The higher effectiveness of w_m as indicator (compared to d_m) is better exemplified in the second row example. Fig. 6 shows the values of $\hat{d}_m = d_m / \max(\mathbf{d})$ and $\hat{w}_m = w_m / \max(\mathbf{w})$ along the contour points of the current shape (being $\mathbf{d} \in \mathbb{R}^M$, $\mathbf{d} = [d_m]$). Note the two local maxima points marked on the plot (contour points 60 and 73) and their representation over the shape contour on Fig. 7 (second row, first column). Concerning $\hat{d}_{60}$ (blue point), v_{60}^b would have higher importance as gripper candidate. However, v_{73}^b (yellow dot) represents a much better candidate as it favours control over the shape's appendix. Fig. 6 gives a better insight on this comparison by showing the results of applying a point-to-point trivial control law ($\mathbf{u}_g = \alpha(\bar{\mathbf{v}}_g^b - \mathbf{v}_g^b)$) for both gripper configurations (in simulation, using ARAP model [19] [20]). More simulations of the point-to-point control law being applied to bad and well conditioned gripper positioning can be visualised on the attached video. In some cases, the local nature of the trivial control law leads to an error increase during the transitory period, even with good gripper configurations (e.g. last simulation). Third row exemplifies how relevant the second term of the optimisation function becomes on shape control tasks involving symmetries. All of the 6 grippers positioned on the first result (column 3) have the same w_m value. The gripper centroid criterion works effectively and allows for a more favourable distribution of grippers. The last two examples are local deformation cases containing straight lines (low descriptor richness) and are properly addressed.

VI. CONCLUSIONS

We have developed a gripper positioning method for multi-robot shape control. A reference deformation process has been proposed considering a fully actuated ideal scenario that allows for a global analysis of the shape evolution over time. Accumulation of multi-scale centroid paths' error over iterations defines our gripper-importance metric. We proved feasibility of centroid points control and thus emphasised the relevance of our gripper importance metric, which serves as input for the gripper location optimisation. Note that models like the one presented in [5], based on decreasing stiffness, are not applicable in this gripper positioning problem as they do not involve a shape matching process that is aware of the target shape. However, it would be interesting to test how our gripper positioning metric interacts with particular control laws from the literature such as [3] or [5]. Our metric could also be tested in cases in which the object's volumetric information is available as the process explained in section III theoretically holds for 3D volumetric objects. Lines and circles would become their 3D analogous (planes and spheres) and the properties of the analogous 3D affine transform $\mathbf{T}$ generalise to 3D as well.

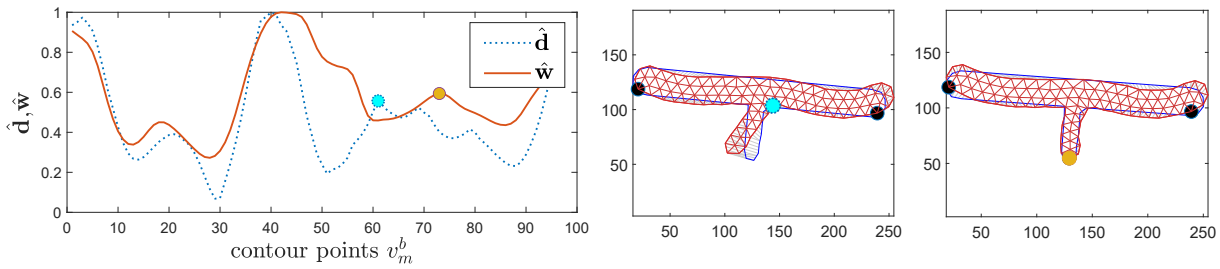

Fig. 6: On the left, comparison of our gripper importance metric ($\hat{\mathbf{w}}$) and an alternative position-error based metric ($\hat{\mathbf{d}}$) along the contour points of the second example in Fig. 7. The results (for last step $k = K$) of applying each metric on simulation (using a trivial point-to-point control law) can be seen on the right, where the blue and yellow points correspond to the local maxima marked on the plot. Note how, unlike $\hat{\mathbf{d}}$, $\hat{\mathbf{w}}$ importance metric allows to control the shape's appendix.

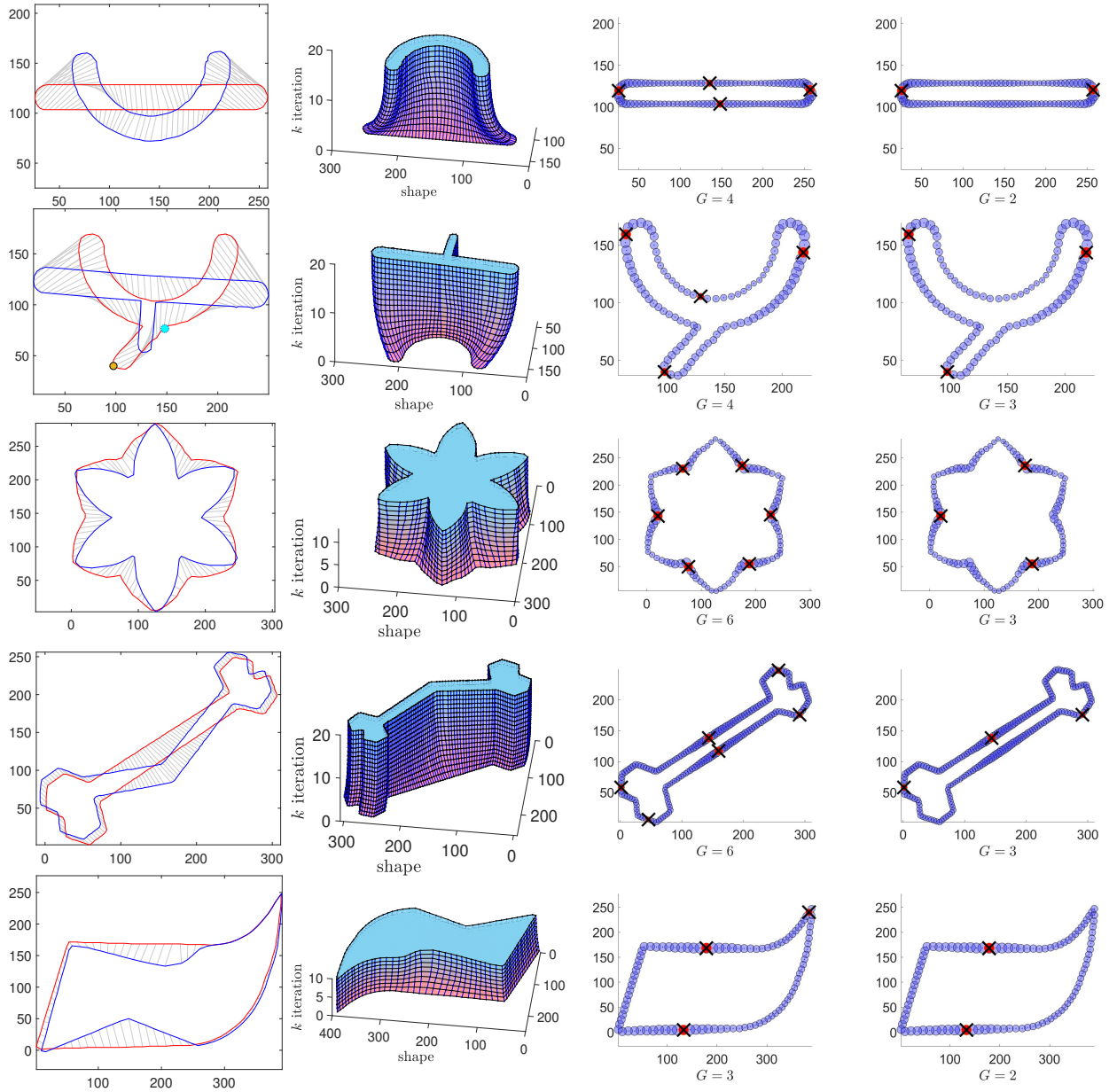

Fig. 7: Results of 5 different cases. First column shows the shape control problem to be solved. Second one the fully-actuated deformation process. The last two columns show gripper positioning results for different number of grippers G (see section V for detailed explanations). The two points on the second example refer to Fig. 6.

REFERENCES

[1] P. Jiménez. Survey on model-based manipulation planning of deformable objects. *Robotics and computer-integrated manufacturing*, 28(2):154–163, 2012.

[2] R. Herguedas, G. López-Nicolás, R. Aragüés, and C. Sagüés. Survey on multi-robot manipulation of deformable objects. In *2019 24th IEEE International Conference on Emerging Technologies and Factory Automation (ETFA)*, pages 977–984, 2019.

[3] D. Navarro-Alarcon, H.M. Yip, Z. Wang, Y.H. Liu, F. Zhong, T. Zhang, and P. Li. Automatic 3-D manipulation of soft objects by robotic arms with an adaptive deformation model. *IEEE Transactions on Robotics*, 32(2):429–441, 2016.

[4] J. Zhu, D. Navarro-Alarcon, R. Passama, and A. Cherubini. Vision-based manipulation of deformable and rigid objects using subspace projections of 2D contours. *Robotics and Autonomous Systems*, 142:103798, 2021.

[5] D. Berenson. Manipulation of deformable objects without modeling and simulating deformation. In *2013 IEEE/RSJ International Conference on Intelligent Robots and Systems*, pages 4525–4532, 2013.

[6] L. Han, H. Wang, Z. Liu, W. Chen, and X. Zhang. Vision-based cutting control of deformable objects with surface tracking. *IEEE/ASME Transactions on Mechatronics*, 26(4):2016–2026, 2021.

[7] M.A. Roa and R. Suárez. Grasp quality measures: review and performance. *Autonomous Robots*, 38(1):65–88, July 2015.

[8] F. Nadon and P. Payeur. Automatic selection of grasping points for shape control of non-rigid objects. In *2019 IEEE International Symposium on Robotic and Sensors Environments (ROSE)*, pages 1–7, 2019.

[9] A. Ramisa, G. Alenya, F. Moreno-Noguer, and C. Torras. Using depth and appearance features for informed robot grasping of highly wrinkled clothes. In *2012 IEEE International Conference on Robotics and Automation*, pages 1703–1708, 2012.

[10] F. Zhang and Y. Demiris. Learning grasping points for garment manipulation in robot-assisted dressing. In *2020 IEEE International Conference on Robotics and Automation*, pages 9114–9120, 2020.

[11] K.-K. Oh, M.-C. Park, and H.-S Ahn. A survey of multi-agent formation control. *Automatica*, 53:424–440, 2015.

[12] J. Cortés and M. Egerstedt. Coordinated control of multi-robot systems: A survey. *SICE Journal of Control, Measurement, and System Integration*, 10(6):495–503, 2017.

[13] J. Alonso-Mora, R. Knepper, R. Siegwart, and D. Rus. Local motion planning for collaborative multi-robot manipulation of deformable objects. In *2015 IEEE international conference on robotics and automation*, pages 5495–5502, 2015.

[14] G. López-Nicolás, R. Herguedas, M. Aranda, and Y. Mezouar. Simultaneous shape control and transport with multiple robots. In *IEEE International Conference on Robotic Computing*, pages 218–225, 2020.

[15] J. Das and N. Sarkar. Autonomous shape control of a deformable object by multiple manipulators. *Journal of Intelligent & Robotic Systems*, 62(1):3–27, 2011.

[16] I. Cuiral-Zueco and G. López-Nicolás. RGB-D tracking and optimal perception of deformable objects. *IEEE Access*, 8:136884–136897, 2020.

[17] L. Han, H. Wang, Z. Liu, W. Chen, and X. Zhang. Visual tracking control of deformable objects with a FAT-based controller. *IEEE Transactions on Industrial Electronics*, 69(2):1673–1681, 2021.

[18] I. Cuiral-Zueco and G. López-Nicolás. Multi-scale laplacian-based FMM for shape control. *In 2021 International Conference on Intelligent Robots and Systems*, pages 3792–3797, 2021.

[19] O. Sorkine and M. Alexa. As-rigid-as-possible surface modeling. In *Symposium on Geometry processing*, volume 4, pages 109–116, 2007.

[20] M. Shetab-Bushehri, M. Aranda, Y. Mezouar, and E. Ozgur. As-Rigid-As-Possible shape servoing. *IEEE Robotics and Automation Letters*, 7(2):3898–3905, 2022.